Smart Structures and Systems, *Vol. 20, No. 5 (2017) 619-636*
DOI: https://doi.org/10.12989/sss.2017.20.5.619

Real-time model updating for magnetorheological damper identification: an experimental study

Wei Song*, Saeid Hayati[a] and Shanglian Zhou[b]

Department of Civil, Construction and Environmental Engineering,
The University of Alabama, Tuscaloosa, AL, USA 35487

(Received July 4, 2017, Revised September 17, 2017, Accepted September 20, 2017)

Abstract. Magnetorheological (MR) damper is a type of controllable device widely used in vibration mitigation. This device is highly nonlinear, and exhibits strongly hysteretic behavior that is dependent on both the motion imposed on the device and the strength of the surrounding electromagnetic field. An accurate model for understanding and predicting the nonlinear damping force of the MR damper is crucial for its control applications. The MR damper models are often identified off-line by conducting regression analysis using data collected under constant voltage. In this study, a MR damper model is integrated with a model for the power supply unit (PSU) to consider the dynamic behavior of the PSU, and then a real-time nonlinear model updating technique is proposed to accurately identify this integrated MR damper model with the efficiency that cannot be offered by off-line methods. The unscented Kalman filter is implemented as the updating algorithm on a cyber-physical model updating platform. Using this platform, the experimental study is conducted to identify MR damper models in real-time, under in-service conditions with time-varying current levels. For comparison purposes, both off-line and real-time updating methods are applied in the experimental study. The results demonstrate that all the updated models can provide good identification accuracy, but the error comparison shows the real-time updated models yield smaller relative errors than the off-line updated model. In addition, the real-time state estimates obtained during the model updating can be used as feedback for potential nonlinear control design for MR dampers.

Keywords: nonlinear model identification; real-time; model updating; magnetorheological (MR) damper; power supply; unscented Kalman filter (UKF)

1. Introduction

After four decades of development, structural control has evolved from a concept (Yao 1972) to a technique with systematic design methods and abundant practical applications (Spencer and Nagarajaiah 2003). Many smart energy dissipation devices have been developed and applied in structural control systems due to their distinctive adjustable or controllable behaviors. These behaviors, often exhibiting highly nonlinear hysteresis, are tuned in real-time by following a control design to generate time-varying physical inputs (e.g., electric current) in response to random loading conditions. However, to achieve the desirable control performance with such a nonlinear device, an accurate model describing its nonlinear controllable behavior is essential. This study presents a real-time nonlinear model updating study on one type of such smart devices—magnetorheological fluid damper ("MR damper" in short), which provides an accurate mathematical model for the MR damper, and the real-time computation environment enables the online estimation of model parameters as feedback for potential nonlinear control design.

As one of the widely studied control devices, the MR damper has shown great promise for seismic protection (Dyke *et al.* 1998). Like many other energy dissipative devices, the MR damper (**A** in Fig. 1) exhibits strong nonlinear behavior. The MR fluid filled in the damper reacts to the surrounding magnetic field by transforming its fluid form with relatively low viscosity to a quasi-solid as the field strength increases. The varying magnetic field is often realized by changing the command voltage signal sent to the power supply unit (PSU) of the damping system (**B** in Fig. 1). To design a reliable control law to accomplish this change, an accurate mathematical model for understanding and predicting the controllable damping force of the MR damper under a wide range of inputs, for both motion and command voltage, is necessary.

Many existing MR damper models have been developed over the years. The commonly used phenomenological model for MR devices is based on the Bouc-Wen model, and was introduced in (Spencer *et al.* 1997). Other models include the Bingham visco-plastic model (Stanway *et al.* 1987), nonlinear hysteretic biviscous model (Wereley and Pang 1998), hyperbolic tangent model (Gavin 2001, Bass and Christenson 2007), modified Bouc-Wen model (Lin *et al.* 2005), viscous plus Dahl model (Rodriguez *et al.* 2009),

*Corresponding author, Assistant Professor
E-mail: wsong@eng.ua.edu
[a] Ph.D. Student
E-mail: shayati@crimson.ua.edu
[b] Ph.D. Student
E-mail: szhou11@crimson.ua.ed

http://www.techno-press.com/journals/sss&subpage=7
ISSN: 1738-1584 (Print), 1738-1991 (Online)

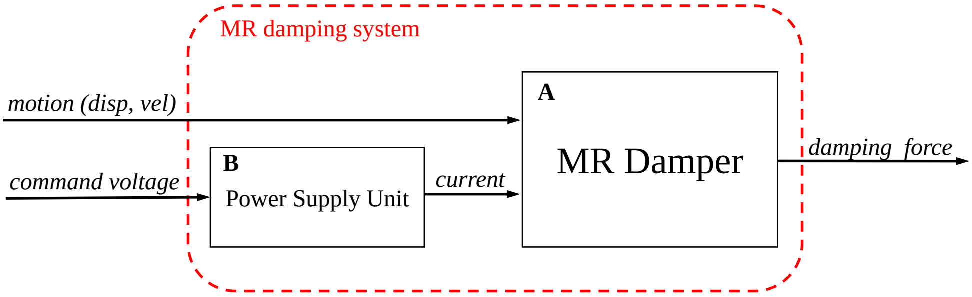

Fig. 1 General block diagram of the integrated MR damping system

and algebraic model (Choi *et al.* 2001, Song *et al.* 2005, Ruangrassamee *et al.* 2006). In (Jiang and Christenson 2011), a study was conducted to compare several MR damper models' stability, convergence, computational time and response prediction in real-time hybrid tests using a large-scale 200 KN MR damper. Typically, these models are calibrated at constant current levels. Then a regression analysis is applied on the calibrated modeling parameters with respect to the corresponding current levels to characterize the tuning effects from current to the damper force. In such a characterization process, a significant amount of data sets, covering a wide range of inputs, need to be analyzed off-line, posing a large computational demand. In addition, the dynamics of the PSU, which is an integrated component in the MR damping system, is often ignored in this characterization process.

This study proposes the use of real-time model updating method for the identification of MR damper as an integrated system, under in-service conditions with random inputs for both motion and command voltage. One of the existing MR damper models, the phenomenological Bouc-Wen model developed in (Spencer *et al.* 1997) is combined with a dynamic model of the PSU as the integrated system model to be identified in this study. The proposed real-time model updating method is based on the unscented Kalman filter (UKF), and is implemented on a cyber-physical platform to conduct the experimental study in real-time computation environment. The experimental study presented in this paper aims to demonstrate the capability of the proposed model updating method in accurately identifying a complex nonlinear model for the integrated MR damper system, but more importantly, doing so in real-time under in-service conditions with time-varying inputs for both motion and command voltage. The electric current applied during the experimental study includes band-limited white noise (BLWN) and random varying signals from clipped-optimal control developed in (Dyke *et al.* 1996), mimicking the working condition of a semi-actively controlled MR damper in the field. To the best of the author's knowledge, this is the first time that the identification of MR damper model is completed under in-service conditions with non-constant current levels. The advantage of the presented nonlinear real-time updating can be seen in these aspects: *i*) providing an accurate nonlinear dynamic model for the complex MR damper behavior in an efficient online manner, reducing the computing time from hours to a few seconds; *ii*) the real-time state estimates obtained under in-service condition can be used as feedback for future nonlinear control design; and *iii*) the integration of the damper and the PSU enables a direct dynamic model from the motion and command voltage inputs to damping force output, and eliminates the need of current measurement in the identification and even control process. These features can enable more robust control design for MR damper in the field. For instance, the requirement of current sensors may be accompanied with a higher chance of failure, noise contamination, and additional cost.

The paper is organized as follows: First, the integrated MR damper model is introduced in section 2, which contains both the phenomenological Bouc-Wen model and a PSU model. Then, the real-time model updating platform is presented in section 3, including both the UKF technique and the real-time updating experimental platform. In the "Experimental Study" section, the real-time updating results obtained under in-service condition (random inputs and clipped-optimal control inputs) are compared with the ones obtained using conventional off-line identification approach. A summary of the results and observations are presented in the end.

2. Integrated MR damper model

The integrated MR damper model (see Fig. 1) describes the damping force (the output) under the varying motion and command voltage (the inputs) is introduced herein. It contains two components: *i*) MR damper model (**A** in Fig. 1) and *ii*) PSU model (**B** in Fig. 1). They are introduced in details in the following sections.

2.1 Modeling for MR damper

MR damper harnesses the behavior of the magneto-rheological (MR) fluid, a type of controllable fluid with the ability to reversibly change from a free-flowing, linear, viscous fluid to a semi-solid when exposed to a magnetic field (Dyke 1996). The MR damper used in study consists of a fixed orifice monotube filled with magneto-rheological fluid as shown in Fig. 2. The main cylinder houses the piston, the magnetic circuit, an accumulator and MR fluid. The MR fluid is a proprietary formulation developed by the Lord Corporation, which has a very low plastic viscosity, and the particle separation and settling do not present any problem. In addition, the monotube chamber has an

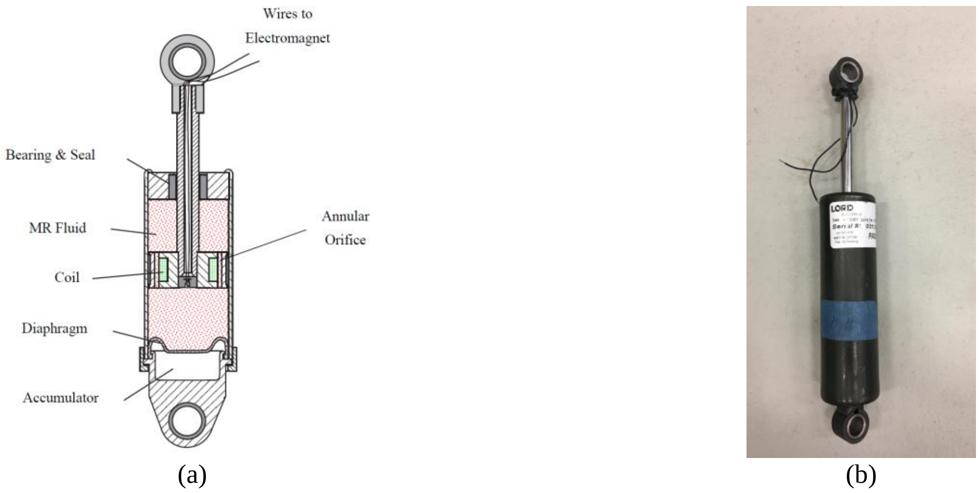

Fig. 2 Schematic (a) and actual picture and (b) of tested MR damper

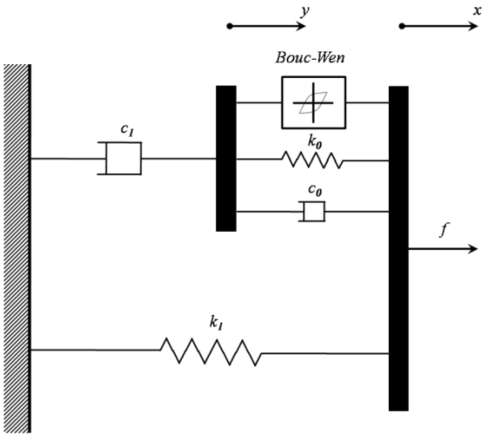

Fig. 3 Schematic of phenomenological MR damper model

accumulator containing high-pressure nitrogen gas (300 psi). The accumulator serves as a volume compensator due to the change in volume available to the fluid caused by: *i*) the piston rod enters the monotube; and *ii*) thermal expansion of the MR fluid.

As mentioned in the "Introduction", many MR damper models have been developed and successfully applied in the structural control community. This study selects one of the most widely used MR damper models, the phenomenological Bouc-Wen model developed in (Spencer *et al.* 1997), as the MR damper model (**A** in Fig. 1).

In this model (shown in Fig. 3), the accumulator stiffness is represented by k_1, the viscous damping observed at larger velocities is related to dashpot, c_0. Another dashpot, represented by c_1, is included in the model to produce the force roll-off at lower velocities. Spring k_0 is applied to control the overall stiffness, and f_0 is the initial damper force due to the accumulator. According to Fig. 3, the forces on either side of the rigid bar are equivalent. Therefore the following equation can be derived

$$\dot{y} = \frac{1}{(c_0 + c_1)}[\alpha z + c_0\dot{x} + k_0(x - y)] \tag{1}$$

Where x and $\dot{x}$ are the motion inputs, in displacement and velocity, on the damper piston, and variables y and z are internal state variables. The Bouc-Wen equation governs the state z

$$\dot{z} = (\dot{x} - \dot{y}) - \beta|\dot{x} - \dot{y}|z|z|^{n-1} - \gamma(\dot{x} - \dot{y})|z|^n \tag{2}$$

The output damping force is given as

$$f = c_1\dot{y} + k_1 x + f_0 \tag{3}$$

This model has 9 parameters (α, β, γ, n, c_0, c_1, k_0, k_1, f_0) and 2 state variables (y, z). Notice from the Bouc-Wen Eq. (2) that the parameter A in the original publication is normalized to 1 to avoid non-unique model parameter sets (Song 2011). Based on the results obtained in the offline identification study shown later (section 4.3), the value of parameter k_1 is close to zero, and therefore it is kept as zero in the real-time updating study. In addition, as a semi-active device, MR damper is not expected to inject energy into the controlled system. This energy related feature can be guaranteed in the modeling of MR damper by reinforcing passivity conditions. In this study, relationship $\beta = \gamma$ is reinforced during the identification process, which leads to the bounded input bounded output (BIBO) property for the phenomenological Bouc-Wen model and subsequently the passivity condition (Ikhouane and Rodellar 2007). The units for the parameters are α (lbf/in), β (in^{-n}), γ (in^{-n}), c_0 (lbf·s/in), c_1 (lbf·s/in), k_0 (lbf/in), f_0 (lbf).

2.2 Modeling for power supply unit

A full-fledged MR damper system requires a companion power supply unit (PSU). In this study, a LORD Wonder Box® device serves as PSU to generate the electric current to the MR damper based on the command voltage input. This device offers both manual and external voltage control modes. For the experiment study conducted in this paper, only external voltage control is used. A photo of the Wonder Box is shown in Fig. 4.

As mentioned in the "Introduction", the behavior of MR damper depends on the strength of the surrounding electromagnetic field, which is in turn determined by the flow of the electric current generated by PSU under command voltage input. In structural control applications, when the current desired by the controller is constant or slowly varying, the dynamic effect of the PSU is not significant, then the desired current can be obtained by converting directly using a proportionate command voltage with a premeasured static gain.

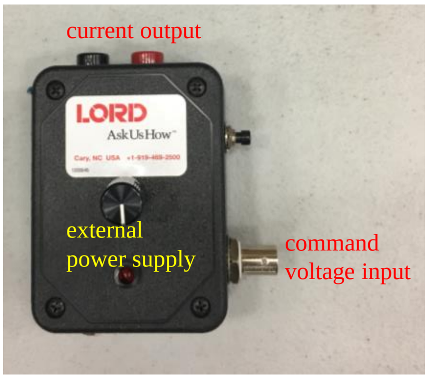

Fig. 4 LORD Wonder Box® power supply unit

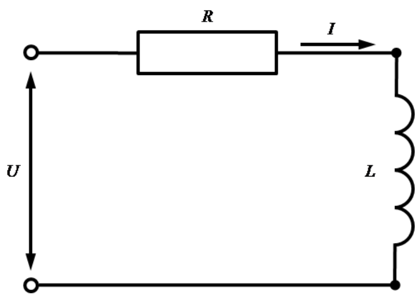

Fig. 5 RL circuit diagram

However, if the desired current levels varies significantly in time, which is often the case given the random nature of the possible inputs (e.g., earthquake, wind) to the structure, a dynamic model (B in Fig. 1) of the PSU is necessary to determine the command voltage signal.

In (Yang 2001), a dynamic model depicts the MR damper electromagnetic circuit for a large-scale 200 KN MR damper was proposed using constant resistance and inductance parameters. Later, Jiang and Christenson (Jiang and Christenson 2012) further improved this model by considering a time-varying inductance due to the strong self-induction effects caused by the large electromagnetic coil in the same 200KN MR damper. In this study, because the MR damper (see Fig. 2) has a much smaller coil comparing to the previous 200KN one, the self-induction caused inductance variation is negligible. A resistor-inductor (RL) circuit model (see Fig. 5) with constant resistance and inductance is applied as the PSU model to describe the dynamic relationship between the command voltage and the generated current. As will be shown later, the model fits the experimental results very well. The PSU model can be expressed as

$$\dot{I} = -\frac{R}{L}I + \frac{1}{L}U \tag{4}$$

where I is the output current and U is the input command voltage; R and L indicate the resistance and inductance of the closed-loop circuit of the MR damping system.

2.3 Integrated model for MR damping system

An integrated model of the entire MR damping system is constructed by *i*) MR damper model (Eqs. (1)-(3)); *ii*) PSU model (Eq. (4)); and, *iii*) relationship between the model parameters and the electric current. The last component, the relationship between the model parameters and the electric current, reflects the change in the behavior of the MR fluid in response to the strength of the surrounding magnetic field. In this study, based on the findings in the off-line identification study shown later (section 4.3), linear equations are adopted herein to describe the relationships between the modeling parameters (α, c_0, c_1) and the current (I). These linear equations are expressed as

$$\alpha(I) = \alpha_a + \alpha_b I \tag{5}$$

$$c_0(I) = c_{0a} + c_{0b} I \tag{6}$$

$$c_1(I) = c_{1a} + c_{1b} I \tag{7}$$

Based on Eqs. (1)-(7) the dynamic model of the integrated MR damping system is described by the following nonlinear state space equations

$$\dot{\mathbf{x}} = \begin{bmatrix} \dot{x}_1 \\ \dot{x}_2 \\ \dot{x}_3 \\ \dot{x}_4 \\ \dot{x}_5 \\ \dot{x}_6 \\ \dot{x}_7 \\ \dot{x}_8 \\ \dot{x}_9 \\ \dot{x}_{10} \\ \dot{x}_{11} \\ \dot{x}_{12} \\ \dot{x}_{13} \\ \dot{x}_{14} \\ \dot{x}_{15} \end{bmatrix} = \begin{bmatrix} \dot{y} \\ \dot{z} \\ \dot{I} \\ \dot{\alpha}_a \\ \dot{\alpha}_b \\ \dot{\beta}(=\dot{\gamma}) \\ \dot{n} \\ \dot{c}_{0a} \\ \dot{c}_{0b} \\ \dot{c}_{1a} \\ \dot{c}_{1b} \\ R \\ L \\ \dot{k}_0 \\ \dot{f}_0 \end{bmatrix} = \begin{bmatrix} \frac{1}{(x_8 + x_9 x_3 + x_{10} + x_{11} x_3)}[(x_4 + x_5 x_3) x_2 + (x_8 + x_9 x_3)\dot{x} + x_{14}(x - x_1)] \\ (\dot{x} - \dot{x}_1) - x_6 |\dot{x} - \dot{x}_1| x_2 |x_2|^{x_7 - 1} - x_6 (\dot{x} - \dot{x}_1)|x_2|^{x_7} \\ -\frac{x_{12}}{x_{13}} x_3 + \frac{1}{x_{13}} U \\ 0 \\ 0 \\ 0 \\ 0 \\ 0 \\ 0 \\ 0 \\ 0 \\ 0 \\ 0 \\ 0 \\ 0 \end{bmatrix} \tag{8}$$

with the output equation for the damping force given as

$$y = f = c_1 \dot{y} + f_0 = (x_{10} + x_{11} x_3)\dot{x}_1 + x_{15} \tag{9}$$

The above state space equations show that the integrated MR damping system can be described by the state vector $\mathbf{x}$. This vector contains a total of 15 state variables, including 3 state variables (y, z, and I) augmented with 12 modeling parameters to facilitate the real-time model updating. This model can fully characterize the integrated MR damping system shown in Fig. 1. The inputs to the system are the motion (displacement— x and velocity— $\dot{x}$) and the command voltage U. The output of the system is the damping force f.

3. Real-time nonlinear model updating platform

A nonlinear real-time model updating platform is presented in this section. It contains both cyber and physical components. The cyber components are the real-time updating algorithm and the real-time computation environment applied in the study, and the physical components are the hardware that enables the implementation of the cyber components and the interface to the MR damping system. Details of the cyber and physical components of the platform are described as follows.

3.1 Unscented Kalman Filter (UKF)

In recent years, many techniques have been developed towards the goal of nonlinear hysteretic model identification, including off-line techniques (Song *et al.* 2009, Song 2011, Song *et al.* 2013); the least squares estimation (LSE) (Smyth *et al.* 1999, Lin *et al.* 2001); the extended Kalman filter (EKF) (Yun and Shinozuka 1980, Hoshiya and Saito 1984, Ghanem and Shinozuka 1995a, 1995b, Yang *et al.* 2006, Song and Dyke 2010); the unscented Kalman filter (UKF) (Wu and Smyth 2007, Chatzi and Smyth 2008, Wu and Smyth 2008, Chatzi *et al.* 2010, Song and Dyke 2010); and particle filter (PF, also known as sequential Monte Carlo methods) (Van der Merwe and Wan 2003, Chatzi and Smyth 2008). Among them, UKF has demonstrated great potential for real-time model updating. The UKF was first proposed by Julier and Uhlmann (Julier *et al.* 1995) and further improved in (Julier 2002). Comparing to EKF, UKF does not require to evaluate Jacobian and Hessian matrices, and has superior accuracy to EKF in approximating the statistics of highly nonlinear systems (Wu and Smyth 2007); furthermore, UKF has the advantage over PF by demanding a much smaller number of sampling points, which provides the necessary computational efficiency for possible real-time applications (Chatzi and Smyth 2008).

Recently, there have been a few UKF applications in off-line estimation of the parameters of nonlinear hysteretic systems (Wu and Smyth 2007, Chatzi and Smyth 2008, Wu and Smyth 2008, Chatzi *et al.* 2010). Song and Dyke (Song and Dyke 2014) have successfully applied UKF to update a nonlinear hysteretic model for a steel mode building subjected to earthquake excitation in real-time. Later, UKF has also been applied in updating nonlinear structural components in hybrid simulation (Hashemi *et al.* 2014, Wu and Wang 2014, Shao *et al.* 2016, Ou *et al.* 2017). Because of its capability and the computational efficiency in nonlinear system estimation, UKF is chosen for conducting the MR damper real-time updating study in this paper. The algorithm is briefly reviewed herein. Consider a general nonlinear dynamical system to be updated

$$\dot{\mathbf{x}} = \mathbf{F}[t, \mathbf{x}(t), \mathbf{u}(t), \mathbf{w}(t)] \tag{10}$$

with the measurement equation at $t = k \cdot \Delta t$ given as

$$\mathbf{y}_k = \mathbf{h}(\mathbf{x}_k, \mathbf{u}_k, \mathbf{v}_k) \tag{11}$$

where $\mathbf{F}$ and $\mathbf{h}$ are nonlinear functions; Δt is the sampling period; $\mathbf{x}_k$ and $\mathbf{u}_k$ are the state vector $\mathbf{x}$ and the measurable system input $\mathbf{u}$ evaluated at time $t = k \cdot \Delta t$; $\mathbf{y}_k$ is the system output at time $t = k \cdot \Delta t$; $\mathbf{w}$ and $\mathbf{v}$ are the process and measurement noise vectors, which are assumed to be zero mean multivariate Gaussian noises with covariance $\mathbf{Q}_k$ and $\mathbf{R}_k$ at $t = k \cdot \Delta t$, respectively.

To implement the UKF, Eq. (10) is converted into discrete time form with the following difference equation

$$\mathbf{x}_{k+1} = \mathbf{f}(k, \mathbf{x}_k, \mathbf{u}_k, \mathbf{w}_k) \tag{12}$$

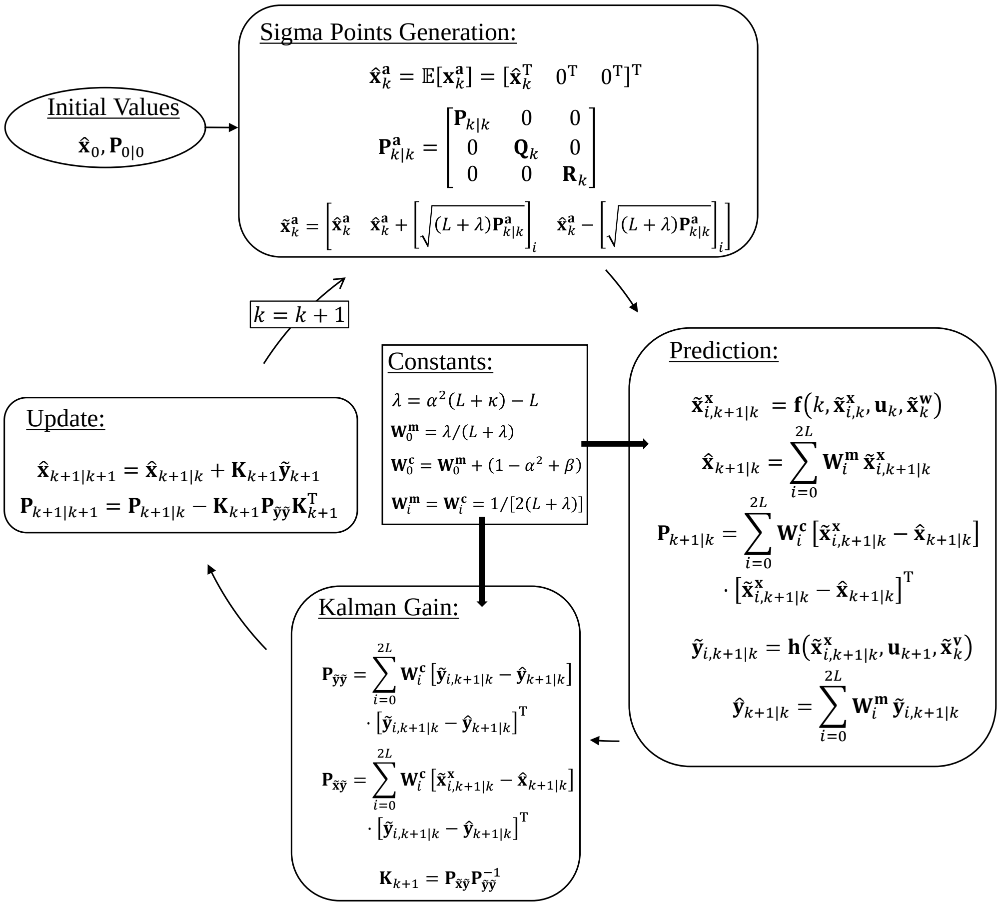

Fig. 6 Flowchart of Unscented Kalman Filter (UKF)

where function $\mathbf{f}$ is obtained by

$$\mathbf{f}(k, \mathbf{x}_k, \mathbf{u}_k, \mathbf{w}_k) = \mathbf{x}_k + \int_{k\Delta t}^{(k+1)\Delta t} \mathbf{F}[t, \mathbf{x}(t), \mathbf{u}(t), \mathbf{w}(t)] \cdot \mathrm{d}t \quad (13)$$

and the integral in Eq. (13) can be evaluated using any suitable time stepping method. However, in the case of real-time computing, an explicit form such as a fourth order Runge-Kutta method is more favorable to avoid the need for iteration in solving the nonlinear equations.

As shown in the flowchart (see Fig. 6), the UKF algorithm has a recursive formulation which contains the following essential steps

1. Sigma Points Generation: Based on the state estimate ($\hat{\mathbf{x}}_k$) and covariance ($\mathbf{P}_{k|k}$) obtained in the previous step ($= k$), a set of $2L + 1$ sampling points $\tilde{\mathbf{x}}_k^{\mathbf{a}}$, namely sigma points, are generated, where L is the dimension of the state vector $\mathbf{x}$.
2. Prediction: The generated sigma points propagate through the nonlinear functions $\mathbf{f}$ and $\mathbf{h}$, and the corresponding sampled mean and variance are used to calculate the predicted state estimate ($\hat{\mathbf{x}}_{k+1|k}$) and estimate covariance ($\mathbf{P}_{k+1|k}$).
3. Kalman Gain: Based on the estimated covariance $\mathbf{P}_{\tilde{\mathbf{y}}\tilde{\mathbf{y}}}$ and $\mathbf{P}_{\tilde{\mathbf{x}}\tilde{\mathbf{y}}}$, the optimal Kalman gain can be obtained as $\mathbf{K}_{k+1}$.
4. Update: The predicted state estimate ($\hat{\mathbf{x}}_{k+1|k}$) and estimate covariance ($\mathbf{P}_{k+1|k}$) are updated using Kalman gain to obtained the updated state estimate ($\hat{\mathbf{x}}_{k+1|k+1}$) and estimate covariance ($\mathbf{P}_{k+1|k+1}$), and then proceed to the next time step.

It can be shown that UKF is accurate to the third order for any nonlinear function $\mathbf{f}$, if the distribution of the original random variable $\mathbf{x}$ is Gaussian. For non-Gaussian $\mathbf{x}$, the approximations are accurate to at least the second order, with the accuracy of third and higher order depending on the parameter setting of UKF.

3.2 Real-time computation environment

The real-time computation environment is an essential component supporting this model updating study. It contains *i*) real-time operating system (RTOS) and *ii*) algorithm development environment (ADE). RTOS is responsible for managing hardware resources, prioritizing tasks and scheduling task executions. ADE provides necessary software support to implement the model updating algorithm—UKF for the real-time execution. In this study, the xPC Target™ and the Simulink Real-Time™ (MATHWORKS 2016) are used to provide the required real-time computation environment:

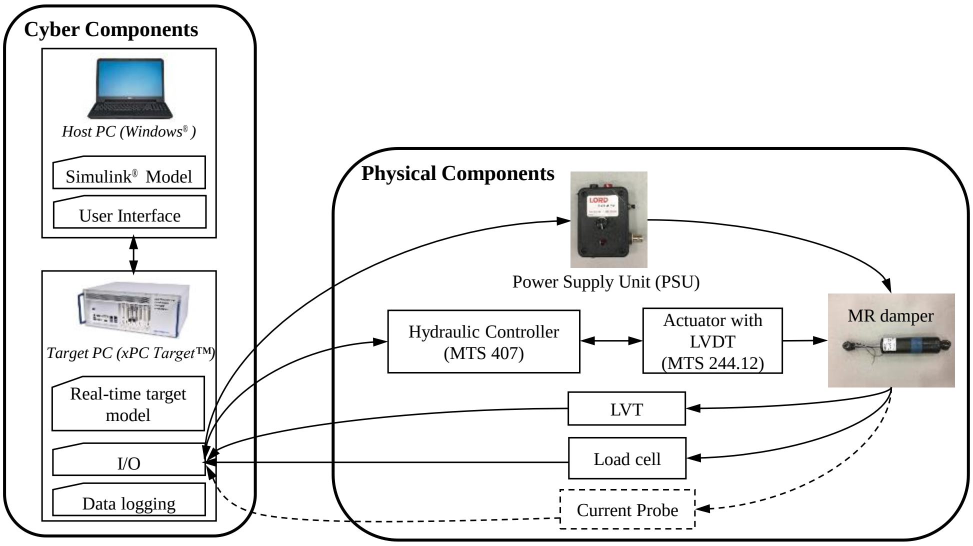

Fig. 7 Schematic of MR damper real-time updating platform

- Simulink Real-Time™ serves as the ADE. The UKF algorithm for MR damper updating is implemented in Simulink model as a custom function block using the Simulink Real-Time™. This process takes place in a "host PC"—a regular laptop that is operated under Windows® environment (see "Host PC" in Fig. 7). Several custom block options are available in Simulink Real-Time™ for this implementation. The one is adopted in this study is the "S-function block" created using C code because of its flexibility in implementing diverse functionalities and a wide range of supporting APIs. Once implemented, the Simulink model is compiled and downloaded to the Target PC.
- xPC Target™ serves as the RTOS. The compiled Simulink model is called "target model", and is downloaded to a target PC operated under "xPC Target™" (see "Target PC" in Fig. 7) for real-time execution. The xPC Target™ coordinates all the computation and connected hardware, and guarantees the precise timing in real-time task execution. In this study, a Speedgoat performance real-time target machine equipped with an Intel core i7 3.5GHz processor and 4 GB or RAM is used as the target PC.

The target PC has a hardware input/output (I/O) interface which establishes the communication between the target machine and other hardware.

3.3 Cyber-physical platform

The UKF and the real-time computation environment introduced above, combined with the necessary hardware required for the MR damper experimental setup, constitute a cyber-physical platform for the real-time model updating experimental study, shown in Fig. 7. The cyber components include the UKF, the real-time computation environment, the necessary computation elements (Host PC and Target PC), and the data acquisition (DAQ) system (as "I/O"). The physical components include the MR damper, PSU, the servo-hydraulic controller and actuator, and sensors (LVDT—Linear Variable Differential Transformer, LVT—Linear Velocity Transducer, load cell and current probe). During the real-time model updating, the motion and command voltage inputs to the MR damping system (shown in Fig. 1) are sent from the I/O of the target PC. The displacement of the damper piston is measured by the internal LVDT inside the actuator, and the damping force generated in the MR damper is measured by the load cell. The velocity is measured by an external LVT. It is noted that the current is also measured by a current probe.

Actually based on Fig. 1 and Eqs. (8) and (9) the current I is one of the state variable not the system output, and therefore is not required to be measured for model updating. However, the current is still measured in this study for the purpose to evaluate the updating results, and therefore the associated signal connections are indicated by dashed lines rather than solid lines in Fig. 7. The details of each physical component will be introduced in the "Experimental Implementation" section later.

4. Experimental study

The real-time nonlinear model updating of the MR damping system is described in this section. First, the experimental setup is presented in details to realize the physical components shown in Fig. 7; then, a MR damper model is identified using conventional off-line technique under sinusoidal motion combined with different levels of constant current; after that, two MR damper models are obtained using the proposed real-time nonlinear updating technique under two in-service conditions: *i*) random motion with random current levels and *ii*) earthquake motion with semi-actively controlled current levels; In the end, the accuracy of the three obtained MR damper models are evaluated using the data obtained under a new set of random motion with random current inputs.

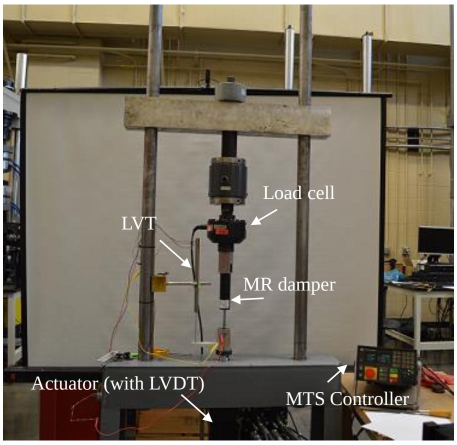

Fig. 8 Experimental setup for MR damper

4.1 Experimental Implementation

The experimental setup shown in Fig. 8 is a realization of the physical components described in Fig. 7. The MR damper used in study (also see Fig. 2) can generate a peak-to-peak damping force of 2447 N (550 lbf) with relatively low power requirement (approx. 1 Amp). The stroke of the damper is 74 mm (2.91 in), with the fully extended length at 248 mm (9.76 in). The main cylinder is 41.3 mm (1.625 in) in diameter. The motion input to the damper is generated by a MTS actuator—model number 244.12, with 5.5 kip force capacity and 6 inch stroke. The controller for the actuator is MTS 407. The displacement input x is measured by the internal LVDT in the actuator, and the signal is sent back to the I/O via the controller. The velocity input $\dot{x}$ is measured by a LVT made by Trans Tek, Inc., with 4 inch stroke and 20 inch/sec limit. The MR damper is connected to a Wonder Box as the PSU (same as shown in Fig. 4), which can generate a maximum current of 2 Amp with a 0-5 Volts DC signal input. The command voltage U is sent to the PSU and measured directly by the I/O. The current level I generated in the closed loop circuit is measured by a current probe manufactured by Tektronix, with the working range from 50 mA to 100A for a frequency bandwidth up to 100 kHz. The force f generated from the damper is measured by a MTS load cell with 2 kip measuring range. With all the inputs (x, $\dot{x}$, U) and outputs (I—only for performance evaluation not for updating, f) of the MR damping system being measured in real-time, the updating platform shown in Fig. 7 can be applied for identifying nonlinear models for MR damper.

Information regarding the noise level is required in the determination of $\mathbf{Q}_k$ and $\mathbf{R}_k$ in the UKF formulation (see Eqs. (10)-(12)). To reduce the noise level in the real-time updating, a low-pass IIR (infinite impulse response) Butterworth filter with cut-off frequency at 30 Hz is applied on all collected channels. In this study, the sampling frequency for the data acquisition and real-time updating is chosen to be 2048 Hz (corresponding to 0.49 ms sampling period). With this sampling frequency and the presented experimental setup, the noise levels of *i*) the actuator displacement measured by the internal LVDT corresponding to variance 4×10^{-8} [in]^2, *ii*) the velocity measured by the LVT corresponding to variance 3×10^{-7} [in/s]^2, *iii*) the command voltage measurement corresponding to variance 1×10^{-9} [V]^2, iv) the force measured by the load cell corresponding to variance 1×10^{-4} [lbf]^2, and, v) the current measured by the current probe corresponding to variance 1×10^{-5} [Amp]^2, are all measured by averaging 24 measurements taken throughout a day. Again, the current measurement is not used in real-time updating and it is only applied to examine the accuracy of the model updating results. Furthermore, to reach real-time performance, the task execution time (TET) for each time step cannot exceed the sampling period 0.49 ms as a timing constraint.

4.2 Error quantification

To evaluate the performance of the updated models, the following three error indices are applied in this study

$$\mathbf{J_1} = \sqrt{\frac{\sum_n \theta_\mathrm{e}^2}{n}} = \mathrm{RMS}(\theta_\mathrm{e}) \tag{14}$$

$$\mathbf{J_2} = \sqrt{\frac{\sum_n \theta_\mathrm{e}^2}{n}} \Bigg/ \sqrt{\frac{\sum_n \theta_\mathrm{m}^2}{n}} = \mathrm{RMS}(\theta_\mathrm{e})/\mathrm{RMS}(\theta_\mathrm{m}) \tag{15}$$

where θ indicates the response to be compared, which can be either the damping force or the current; $\theta_\mathrm{e} = \theta_\mathrm{s} - \theta_\mathrm{m}$ is the error between the response simulated by the updated model θ_s and the measured response θ_m; and, n indicates the time index of the data. $\mathbf{J_1}$ is considered as an absolute measure of the updating error, whereas $\mathbf{J_2}$ is considered as relative updating errors in the RMS measure.

For both indices, the lower the value, the better the updating results.

4.3 Sinusoidal displacement with constant voltage (current) inputs—off-line identification

Before applying the real-time model updating, the conventional off-line technique under sinusoidal motion

Table 1 Identified model under constant voltage/current

α_a	α_b	$\beta=\gamma$	n	c_{0a}	c_{0b}	c_{1a}	c_{1b}	k_0	f_0
8732.34	22081.83	9123.84	1.69	5.73	14.46	30.69	250.63	26.55	29.31

Table 2 Identified model under random inputs

α_a	α_b	$\beta=\gamma$	n	c_{0a}	c_{0b}	c_{1a}	c_{1b}	R	$L(\times 10^{-3})$	k_0	f_0
12715.09	33394.96	20907.19	1.86	8.80	6.87	88.88	185.99	2.29	4.10	43.86	31.77

combined with different levels of constant current is applied to obtain a MR damper model. This section briefly explains this process and shows the obtained damper model for further comparison later.

A total number of 72 tests are conducted to generate data sets that can cover a range of motion and current inputs. The sinusoidal displacement inputs are excitations with amplitudes of 0.3in, 0.4in, and 0.5in; frequencies of 2Hz, 3Hz, 4Hz, and 5Hz; command voltage inputs 0.5V, 1V, 1.5V, 2V, 2.5V and 3V, corresponding to (approximately) the constant current level 0A, 0.2A, 0.4A, 0.6A, 0.8A and 1A, respectively. The duration for each test is 20 seconds. For each of the test under constant voltage, the parameters of the phenomenological Bouc-Wen model given by the Eqs. (1)-(3) are determined by using the fmincon function in MATLAB (MATHWORKS 2016). This function minimizes the root mean square error (RMSE) between the measured force and the force obtained using the model. The following initial values are chosen

$$\begin{aligned}\hat{\mathbf{x}}_0 &= [y \quad z \quad \alpha \quad \beta(=\gamma) \quad n \quad c_0 \quad c_1 \quad k_0 \quad k_1 \quad f_0]^{\mathrm{T}} \\ &= [0 \quad 0 \quad 2\times 10^4 \quad 2\times 10^4 \quad 1 \quad 50 \quad 200 \quad 100 \quad 10 \quad 10]^{\mathrm{T}}\end{aligned} \tag{16}$$

It takes between 15 to 30 minutes to complete the optimization run for one test case. After the total 72 sets of parameters identified, regression analysis is conducted to obtain the relationship between each parameter and the current level. Simple linear relations have been observed for parameters α, c_0, c_1, which is consistent with the findings in (Spencer *et al.* 1997). Therefore, the linear equations (Eqs. (5)-(7))are used to model the current dependent behavior of these parameters. However, parameters β (which is set to be equal to γ), k_0, k_1 and f_0 are not sensitive to the current change, and therefore are considered as constants in the MR damper model. Furthermore, the value of parameter k_1 is close to zero, and therefore it is kept as zero in the real-time updating study later. It is also noted that in the above off-line identification process, the model obtained is for the MR damper only, and no modeling parameters related to the PSU is identified. In other words, the dynamics of the PSU is ignored in the off-line updating process. The identified MR damper model is shown in Table 1.

4.4 Random displacement with random voltage (current) inputs

In this case, bandlimited white noises (BLWNs) are applied as the displacement input to the damper and the command voltage to the PSU, to simulate one of the two in-service conditions considered in this study. The displacement input to the damper is a bandlimited white noise (BLWN) with maximum amplitude of 0.5 inch and frequency bandwidth of 0-5 Hz. The command voltage to the PSU is another BLWN with frequency bandwidth of 0-15 Hz and amplitude between 0.5V and 3V, similar range as the constant current levels in the previous off-line identification case. The duration of the test is 60 seconds, and the parameters of the MR damping system are updated using the cyber-physical platform in real-time as the test progresses.

For the real-time updating, the UKF is applied by replacing system Eqs. (10) and (11) with the MR damping system model— Eqs. (8) and (9) To start the updating process descried in Fig. 6, the following initial values are chosen

$$\begin{aligned}\hat{\mathbf{x}}_0^{\mathbf{a}} &= [y \quad z \quad I \quad \alpha_b \quad \alpha_b \quad \beta(=\gamma) \quad n \quad c_{0a} \quad c_{0b} \quad c_{1a} \quad c_{1b} \quad R \quad L \quad k_0 \quad f_0]^{\mathrm{T}} \\ &= [0 \quad 0 \quad 0 \quad 2\times 10^4 \quad 4\times 10^4 \quad 2\times 10^4 \quad 1 \quad 10 \quad 10 \quad 100 \quad 200 \quad 1 \quad 10^{-3} \quad 100 \quad 10]^{\mathrm{T}}\end{aligned} \tag{17}$$

and, the corresponding initial covariance matrix is chosen as

$$\mathbf{P}_{0|0}^{\mathbf{a}} = diag([0.1 \quad 0.1 \quad 0.1 \quad 2\times 10^7 \quad 3\times 10^7 \quad 1.5\times 10^7 \quad 0.01 \quad 10 \quad 10 \quad 10^3 \quad 2\times 10^3 \quad 1 \quad 10^{-6} \quad 10^3 \quad 50]) \tag{18}$$

In the above formulation, $diag(\mathbf{x})$ indicates a square diagonal matrix with the elements in vector $\mathbf{x}$ on its main diagonal. It is noted that different choices of initial values for the state variable $\hat{\mathbf{x}}_0^{\mathbf{a}}$ and covariance $\mathbf{P}_{0|0}^{\mathbf{a}}$ may affect the convergence of the UKF algorithm. The selection of the most appropriate set of initial values is out of the scope of this study. The above initial values $\hat{\mathbf{x}}_0^{\mathbf{a}}$ are selected to have the same or similar order of magnitude of the corresponding off-line updated model (see Table 1), except the parameters R and L for the PSU model. Based on the selected $\hat{\mathbf{x}}_0^{\mathbf{a}}$ values, the choice of the initial covariance values $\mathbf{P}_{0|0}^{\mathbf{a}}$ is made by ensuring the corresponding coefficient of variation for each parameter is within the range between 0.1 and 1. Furthermore, the covariance matrices $\mathbf{Q}_k$ and $\mathbf{R}_k$ are determined using the measured noise levels described in section 4.1.

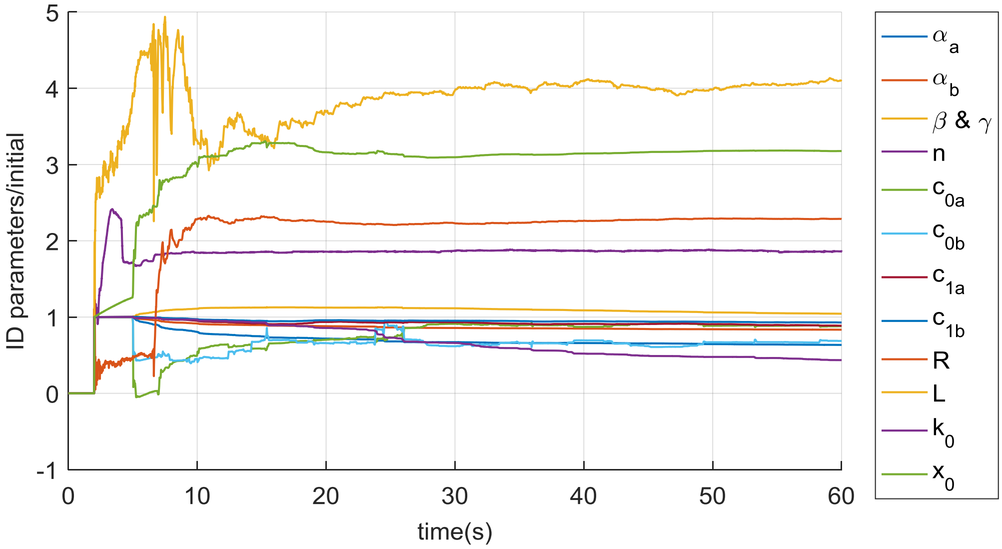

Fig. 9 Updating history of model parameters—random inputs

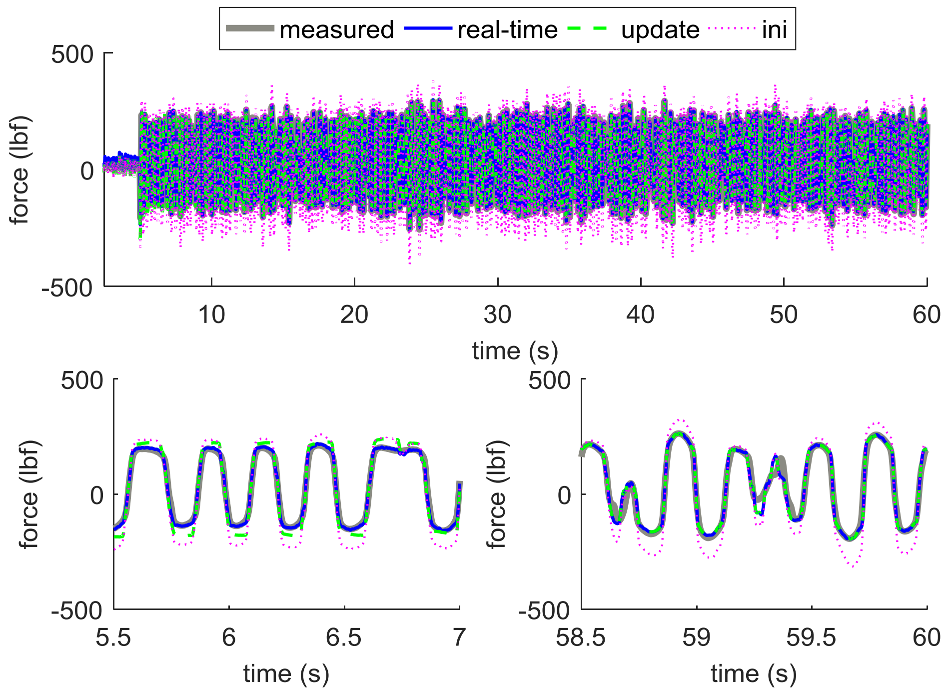

Fig. 10 Comparison of damping force time history—random inputs

The time history of the updated parameter values are shown in Fig. 9. The vertical axis indicate the value of each parameter normalized by the corresponding initial value.

The jump at $t = 2$ seconds is due to switching on the real-time model updating platform. Based on the evolution of the time history, it can be seen that although the different parameters have different convergence speed, most of the parameters reach a stable value after 30 seconds. The updated model parameters are shown in Table 2.

To demonstrate the updating performance, the updated damping force and current are compared with the measured values in Figs. 10 and 11. In each figure, the 'real-time' and 'ini' curves indicate the results obtained using the real-time updated model (see Table 2) and the initial model (see Eq. (17)), respectively. The 'measured' curve indicates the actual damping force and current measurements. The 'update' curve indicates the results obtained during the real-time updating process. Two zoomed-in plots are provided for the beginning stage and the end stage of the real-time updating process. Based on the results shown in these two figures, it is clear to see the 'real-time' curves agree very well with the actual measurements, whereas the results

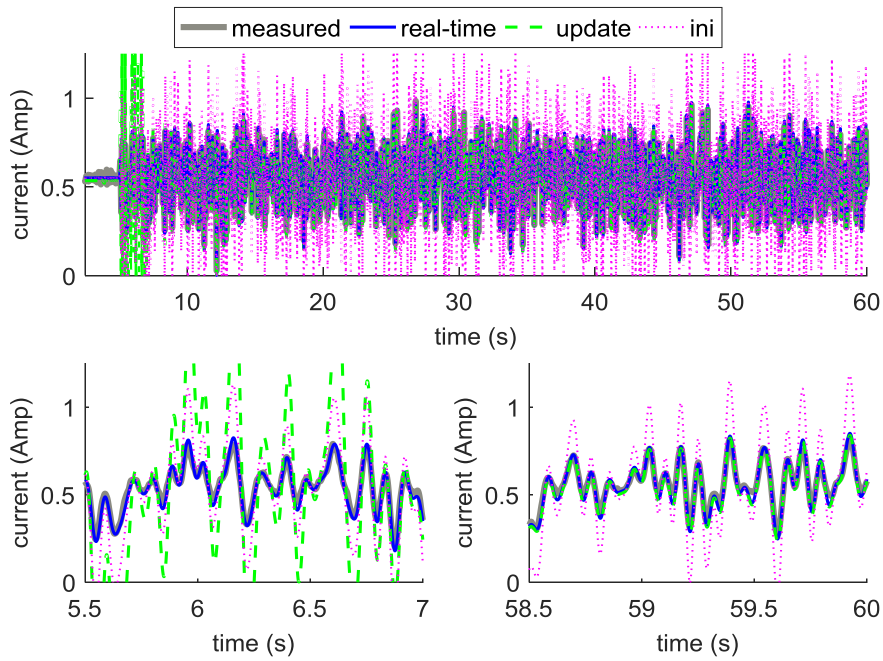

Fig. 11 Comparison of current time history—random inputs

obtained by the initial model yields large error. In addition, the 'update' curves converge to the 'real-time' curve, and matches the actual 'measured' curve in the end. The average and maximum TET are 0.42 ms and 0.46 ms, which satisfy the real-time computing constraint of 0.49 ms.

The error comparison are summarized in Table 3. In the table, the error indices for both the damping force and current are calculated for real-time updated model (Table 2), off-line updated model (Table 1), and the initial model (Eq. (17)). Both the real-time and off-line updated models can provide good accuracy for damping forces. And the real-time updated model shows better results in $\mathbf{J_2}$ than the off-line updated model, possibly because the off-line update model ignores the dynamic behavior of the PSU.

Furthermore, the off-line updated model needs current measurement as an additional input, but the real-time updated model only requires force measurement and can successfully update the PSU model as indicated by a less than 2% error in the obtained current.

4.5 Motion and voltage inputs under earthquake excitation

In this real-time updating case, the motion and command voltage inputs to the MR damper are obtained under a simulated structural control application. For the two-story shear building shown in Fig. 12, the two natural frequencies are 1.1 Hz and 2.8 Hz, respectively. It is assumed that the MR damper is installed on the first floor of the building and the building is subjected to El Centro earthquake record. The motion input to the damper is the relative motion of the first floor with respect to the ground motion. The clipped-optimal control (Dyke *et al.* 1996) is applied to generate the command voltage input with]minimum amplitude and maximum amplitude of 0.5V and 3V, respectively. This case is also used to examine the real-time updating performance when the MR damper is under in-service condition. The duration of the test is 45 seconds. The updated model parameters are shown in Table 4, and the time history of the updated parameter values are shown in Fig. 13. In this case, the average and maximum TET are 0.41 ms and 0.46 ms, which satisfy the real-time computing constraint of 0.49 ms.

For the real-time updating, the initial values for the state variable $\hat{\mathbf{x}}_0^{\mathbf{a}}$ and covariance $\mathbf{P}_{0|0}^{\mathbf{a}}$ are the same as the previous real-time updating case (Eqs. (17) and (18)). The updated damping force and current are compared with the measured values in Figs. 14 and 15. Similar as the results obtained from the previous case with random inputs, the 'real-time' curves agree well with the 'measured' curves for both the damping force and current, indicating good updating accuracy. The 'update' curves reveals how the updating history is improved and finally converge to the 'real-time' curves and the 'measured' curves. The error comparison results are summarized in Table 5. It is noted that again the real-time updated model yields the least error for both damping force and current. Particularly, the error index $\mathbf{J_2}$ of the current for the initial model is close to 50%, but the corresponding $\mathbf{J_2}$ for the real-time updated model is only 7%, indicating a significant improvement in accuracy.

Table 3 Error comparison under random inputs

Error Index	Damping Force (lbf)			Current (Amp)	
	Real-time	Off-line	Initial	Real-time	Initial
$\mathbf{J_1}$	9.79	14.68	61.97	0.01	0.16
$\mathbf{J_2}$	0.06	0.09	0.38	0.02	0.28

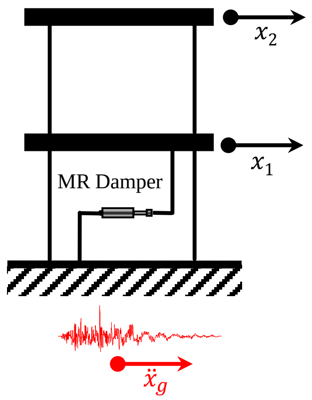

Fig. 12 Two-story shear building under ground motion

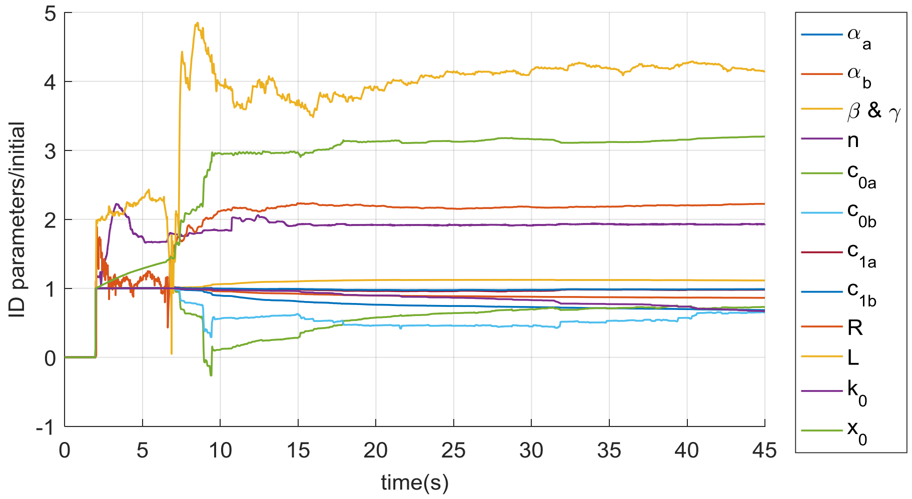

Fig. 13 Updating history of model parameters— earthquake excitation

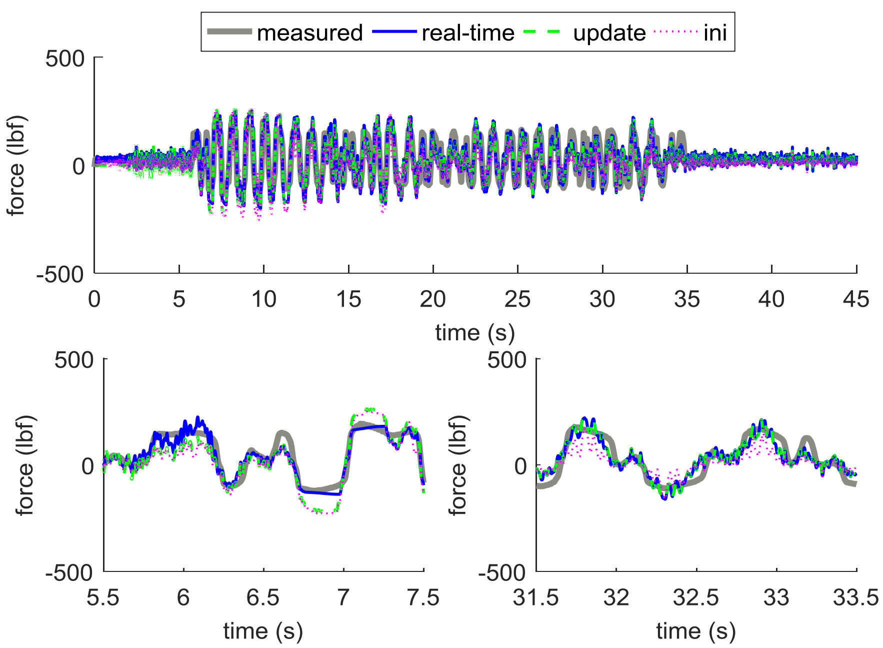

Fig. 14 Comparison of damping force time history—earthquake excitation

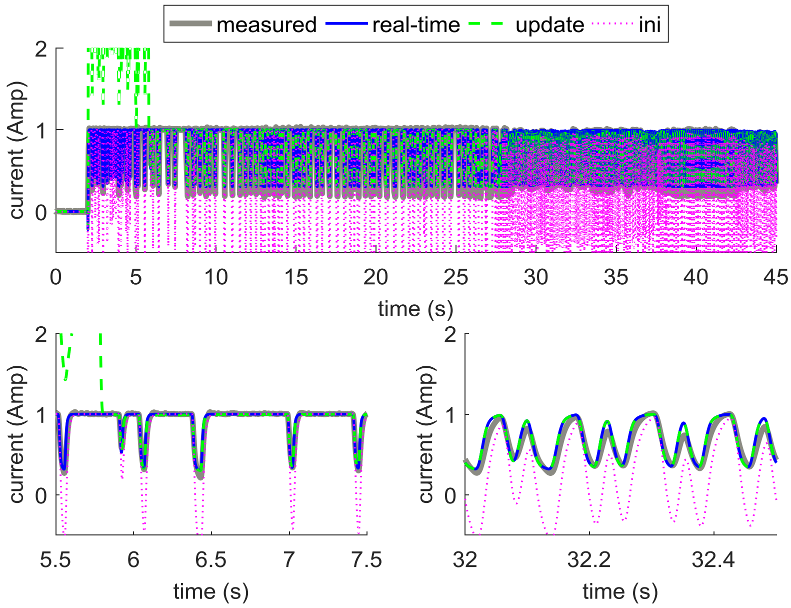

Fig. 15 Comparison of current time history—earthquake excitation

Table 4 Identified model under earthquake excitation

α_a	α_b	$\beta=\gamma$	n	c_{0a}	c_{0b}	c_{1a}	c_{1b}	R	$L(\times 10^{-3})$	k_0	f_0
13735.48	34512.06	22296.03	1.93	7.24	6.48	97.89	197.23	2.20	4.17	67.75	31.95

Table 5 Error comparison under earthquake excitation

Error Index	Damping Force (lbf)			Current (Amp)	
	Real-time	Off-line	Initial	Real-time	Initial
$\mathbf{J_1}$	13.27	15.68	51.87	0.05	0.37
$\mathbf{J_2}$	0.11	0.13	0.43	0.07	0.48

However, in general, the errors obtained in this case are slightly higher than those shown in Table 3. It is likely due to the challenge of a wider frequency bandwidth in the generated current as a result of quickly switching between the minimum and maximum voltage commands during the clipped-optimal control.

4.6 Comparison test (Random inputs)

The final case is to evaluate the accuracy of the previously identified MR damper models under a new set of random inputs (different than the random inputs used for section 4.4). The displacement input is a BLWN with maximum amplitude of 0.5 inch and frequency bandwidth of 0-5 Hz. The command voltage to the PSU is another BLWN with frequency bandwidth of 0-15 Hz and amplitude between 0.5V and 3V. Using the obtained experimental data, the damping force and current obtained from the following models are compared: real-time updated model under random inputs (rt-rnd-rnd) from Table 2; real-time updated model under earthquake excitation (rt-eq-co) from Table 4; off-line updated model under constant voltage (off-sin-const) from Table 1 (with additional current measurement); and initial model (ini) from Eq. (17).

The comparison of the damping forces and currents are shown in Figs. 16 and 17, respectively. From these two figures, it can be seen that the initial model generates large errors throughout the entire time history for both damping force and current, and all the other three updated models provide good visual match to the measured results. The force versus displacement and force versus velocity plots are also shown in Fig. 18. Similar conclusion can be drawn from this figure that all the updated models (real-time and off-line) can capture the nonlinear hysteretic behavior of the MR damper very well, but the initial model produces large amount of error.

To examine the accuracy of the identified PSU model, the experimental transfer function between the command voltage input U and the current output I is obtained. Then, an optimization procedure is conducted to find the optimal R and L values that can best fit the obtained transfer function. This 'optimal' transfer function is compared with the PSU model from the real-time updated models in Fig. 19. The initial model is also included in the same figure. The comparison shows that both real-time updated models have capture the dynamic model of the PSU. Moreover, the good agreement between the models and the experimental transfer function indicates that the RL circuit model assumption (Eq. (4)) fits well with the actual dynamic behavior of the PSU.

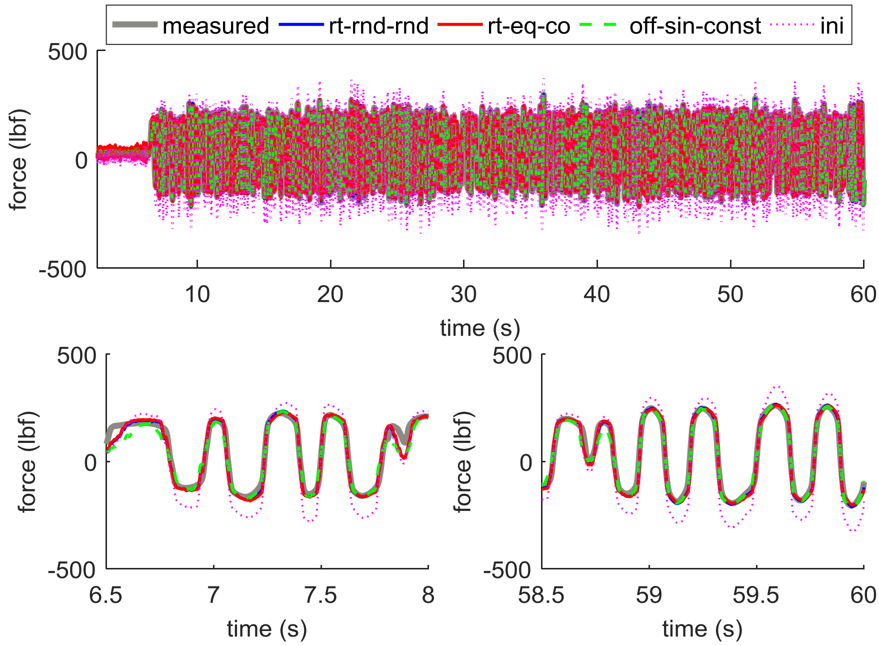

Fig. 16 Comparison of damping force time history

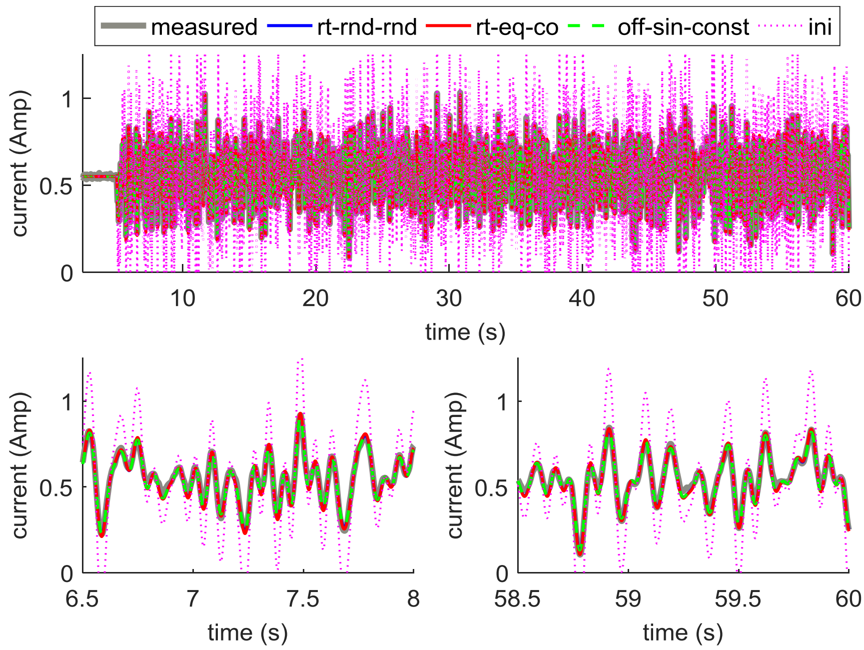

Fig. 17 Comparison of current time history

The error comparison results are summarized in Table 6. It is shown that, all three updated models can provide good identification accuracy with $\mathbf{J_2}$ around 10%. The two real-time updated models offer similar performances but are better than the off-line updated model, possibly because the off-line updated model does not consider the dynamic behavior of the PSU. In addition, for the real-time updated models, the one updated under random inputs (rt-rnd-rnd) yields slightly smaller error than the one updated under earthquake excitation (rt-eq-co). The reason may be that the new set of inputs is of the similar type (amplitude and frequency range) as the inputs used in updating rt-rnd-rnd. Another interesting observation is, although the real-time updated model parameters are very different than the ones in the off-line updated model—some of the parameters, such as $\beta(=\gamma)$, c_{1a}, can be more than 100% apart, the obtained damping forces and currents are very close when comparing to the measured values.

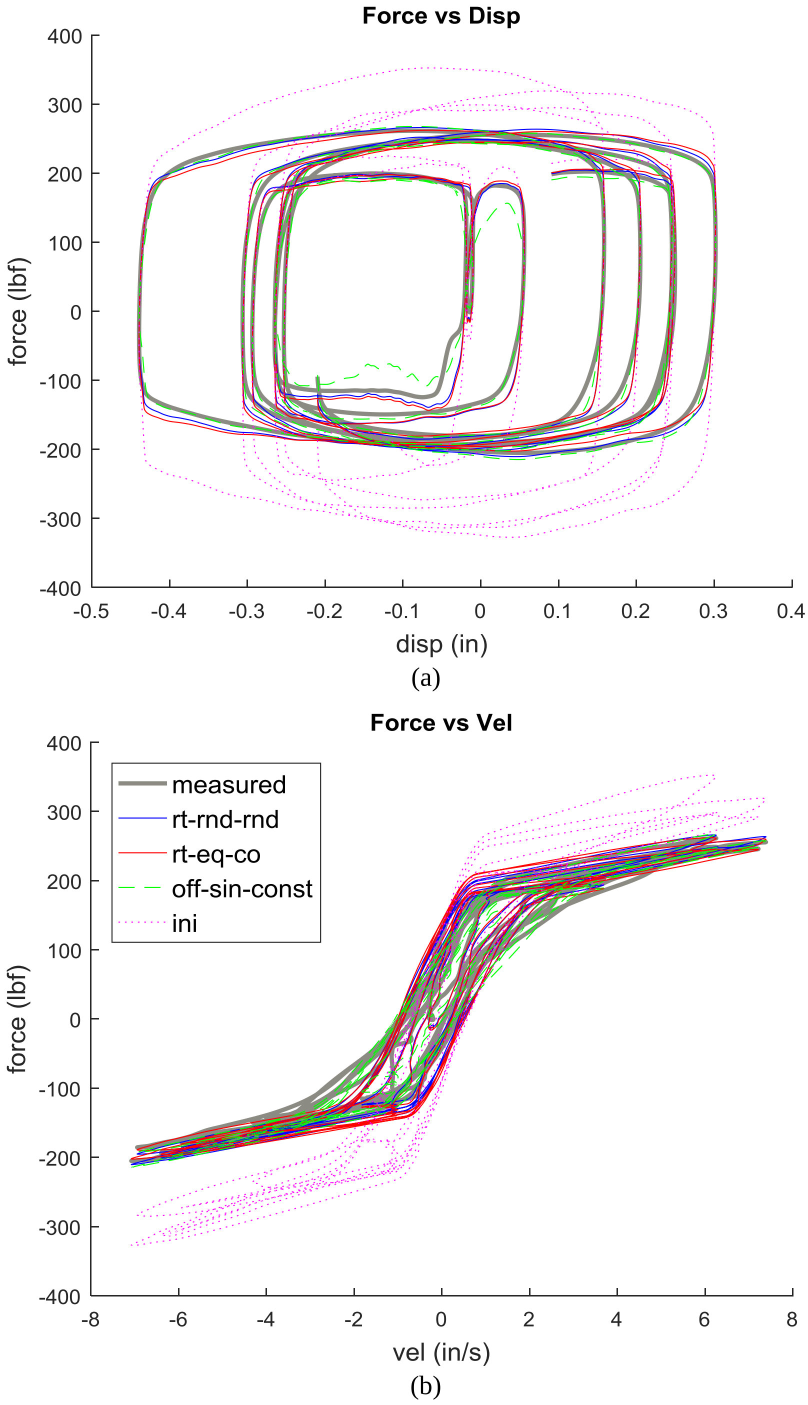

Fig. 18 Comparison of the MR damper responses: (a) force versus displacement and (b) force versus velocity

A possible explanation is that the phenomenological Bouc-Wen model may be overparameterized for modeling the behavior of this MR damper.

The authors also have conducted the real-time updating for the case where only the MR damper model (**A** in Fig. 1) is present. In that case, due to removal of the PSU model (**B** in Fig. 1), the current (I) is no longer a state variable as shown in Eq. (8), but rather a system input that needs to be measured. The corresponding updated model (without the PSU model) obtained under the same inputs as the section 4.4 is also examined herein. The results show that this updated model yields $\mathbf{J_1}$=11.26 and with $\mathbf{J_2}$=0.07, very similar to the accuracy obtained by the rt-rnd-rnd model as shown in Table 6. This comparison result indicates that, even without the current measurement, the real-time updating technique can successfully identify the MR damper parameters with the similar accuracy as the case where the current is measured.

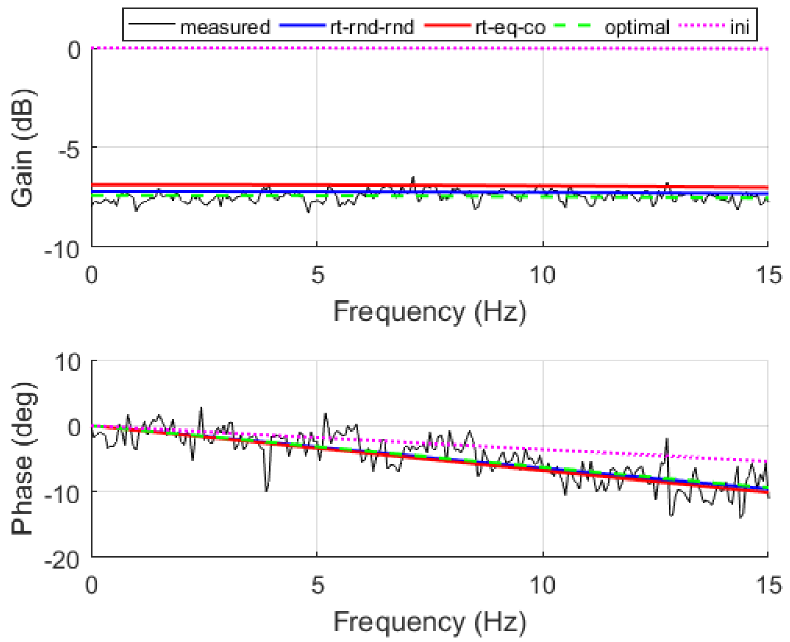

Fig. 19 Transfer function comparison

Table 6 Error comparison

Error Index	Damping Force (lbf)				Current (Amp)		
	rt-rnd-rnd	rt-eq-co	Off-line	Initial	rt-rnd-rnd	rt-eq-co	Initial
J_1	11.73	13.40	18.43	67.01	0.01	0.03	0.20
J_2	0.07	0.08	0.11	0.40	0.02	0.05	0.31

5. Conclusions

This paper presents an experimental study to identify an integrated MR damper model using real-time updating technique. The integrated MR damper model includes a RL circuit model to capture the dynamic behavior of the power supply unit, which is often ignored in off-line identification process. The presented real-time updating technique has the following advantages:

i) Identify accurate nonlinear dynamic model for the complex MR damper behavior in an efficient online manner, reducing the required computing time from hours to seconds.

ii) The real-time state estimates for the MR damper model can be obtained under in-service conditions with time-varying current levels, and therefore can be used as feedback for future nonlinear control design; and,

iii) The integration of the damper and the PSU enables a direct dynamic model from the motion and command voltage inputs to damping force output, and eliminates the need of electric current measurement in the identification and even control process.

In the experimental study, both off-line and real-time model identifications are conducted. The off-line identification is performed using conventional method under constant voltage/current levels; whereas the real-time identifications are conducted using the UKF under in-service conditions with time-varying current levels. The real-time updating experiments are conducted via the nonlinear real-time model updating platform presented. The TETs obtained during the tests are all lower than the timing constraint of 0.49 ms, indicating successful real-time applications.

From the experimental results, especially the comparison among all the updated models, it is shown that all the updated models (real-time and off-line) can provide good identification accuracy. But the two real-time updated models offer better performances (<10% in $\mathbf{J_2}$) than the off-line updated model, possibly because the off-line updated model does not consider the dynamic behavior of the power supply unit. Similar updating performance has been observed by comparing the above updating results with the ones obtained using the case without the PSU model. This indicates that, even without the current measurement, the real-time updating technique can successfully identify the MR damper parameters with the similar accuracy as the case where the current is measured. In addition, multiple updated models have been identified for the same system indicates parameter redundancies in the MR damper model. Further research is necessary to investigate this issue.

References

Bass, B.J. and Christenson, R.E. (2007), "System ientification of a 200 kN mgneto-reological fuid dmper for sructural cntrol in lrge-sale sart sructures", *Proceedings of the 2007 American Control Conference*, New York City, USA.

Chatzi, E.N. and Smyth, A.W. (2008), "The unscented kalman filter and particle filter methods for nonlinear structural system identification with non-collocated heterogeneous sensing", *Struct. Control Health.*, **16**(1), 99-123.

Chatzi, E.N., Smyth, A.W. and Masri, S.F. (2010), "Experimental application of on-line parametric identification for nonlinear Hysteretic Systems with Model Uncertainty", *Struct. Saf.*, **32**(5), 326-337.

Choi, S., Lee, S. and Park, Y. (2001), "A hysteresis model for the field-dependent damping force of a magnetorheological damper", *J. Sound Vib.*, **245**(2), 375-383.

Dyke, S.J. (1996), "Acceleration feedback control strategies for active and semi-active control systems: modeling, algorithm development, and experimental verification", Ph.D. Dissertation, Notre Dame University, Indiana.

Dyke, S.J., Spencer Jr., B.F., Sain, M.K. and Carlson, J.D. (1996), "Modeling and control of magnetorheological dampers for seismic response reduction", *Smart Mater. Struct.*, **5**(5), 565-575.

Dyke, S.J., Spencer Jr., B.F., Sain, M.K. and Carlson, J.D. (1998), "An experimental study of MR dampers for seismic protection", *Smart Mater. Struct.*, **7**(5), 693-703.

Gavin, H.P. (2001), "Multi-duct ER Dampers", *J. Intel. Mat. Syst. Struct.*, **12**(5), 353-366.

Ghanem, R. and Shinozuka, M. (1995a), "Structural System Identification. I: Theory", *J. Eng. Mech.*, **121**(2), 255-264.

Ghanem, R. and Shinozuka, M. (1995b), "Structural System Identification. II: Experimental Verification", *J. Eng. Mech.*, **121**(2), 265-273.

Hashemi, M.J., Masroor, A. and Mosqueda, G. (2014), "Implementation of online model updating in hybrid simulation", *Earthq. Eng. Struct. D.*, **43**(3), 395-412.

Hoshiya, M. and Saito, E. (1984), "Structural identification by extended kalman filter", *J. Eng. Mech.*, **110**(12), 1757-1772.

Ikhouane, F. and Rodellar, J. (2007), *Systems with Hysteresis: Analysis, Identification and Control Using the Bouc-Wen Model*, Wiley-Interscience.

Jiang, Z. and Christenson, R. (2011), "A comparison of 200 kN magneto-rheological damper models for use in real-time hybrid simulation pretesting", *Smart Mater. Struct.*, **20**(6), 1-11.

Jiang, Z. and Christenson, R.E. (2012), "A fully dynamic magneto-rheological fluid damper model", *Smart Mater. Struct.*, **21**(6), 065002 (065012pp).

Julier, S.J., Uhlmann, J.K. and Durrant-Whyte, H.F. (1995), "A new approach for filtering nonlinear systems", *Proceedings of the 1995 American Control Conference*, Seattle, Washington.

Julier, S.J. (2002), "The scaled unscented transformation", *Proceedings of the 2002 American Control Conference*, Anchorage, AK.

Lin, J.W., Betti, R., Smyth, A.W. and Longman, R.W. (2001), "On-line identification of non-linear hysteretic structural systems using a variable trace approach", *Earthq. Eng. Struct. D.*, **30**(9), 1279-1303.

Lin, P.Y., Roschke, P. and Loh, C.H. (2005), "System identification and real application of a smart magneto-rheological damper", *Proceedings of the 2005 IEEE International Symposium on Intelligent Control*, Limassol, Cyprus.

MATHWORKS (2016), *Manual of MATLAB*, MATHWORKS.

Ou, G., Dyke, S.J. and Prakash, A. (2017), "Real time hybrid simulation with online model updating: An analysis of accuracy", *Mech. Syst. Signal. Pr.*, **84B**, 223-240.

Rodriguez, A., Iwata, N., Ikhouane, F. and Rodellar, J. (2009), "Model identification of a large-scale magnetorheological fluid damper", *Smart Mater. Struct.*, **18**(1), 1-12.

Ruangrassamee, A., Srisamai, W. and Lukkunaprasit, P. (2006), "Response mitigation of the base Isolated benchmark building by semi-active control with the viscous-plus-variable-friction damping force algorithm", *Struct. Control Health.*, **13**(2-3), 809-822.

Shao, X., Mueller, A. and Mohammed, B.A. (2016), "Real-time hybrid simulation with online model updating: methodology and implementation", *J. Eng. Mech.*, **142**(2), 04015074-04015071-04015019.

Smyth, A.W., Masri, S.F., Chassiakos, A.G. and Caughey, T.K. (1999), "On-line parameteric identification of MDOF nonlinear hysteretic systems", *J. Eng. Mech.*, **125**(2), 133-142.

Song, W., Dyke, S., Yun, G. and Harmon, T. (2009), "Improved damage localization and quantification using subset selection", *J. Eng. Mech.*, **135**(6), 548-560.

Song, W. and Dyke, S.J. (2010), "Application of nonlinear observers in hysteretic model updating", *Proceeding of SPIE, Sensors and Smart Structures Technologies for Civil, Mechanical, and Aerospace Systems 2010*, San Diego, CA, USA

Song, W. (2011), "Dynamic model updating with applications in structural and damping systems: from linear to nonlinear, from off-line to real-time", Ph.D. Dissertation, Purdue University, Indiana.

Song, W., Dyke, S. and Harmon, T. (2013), "Application of nonlinear model updating for a reinforced concrete shear wall", *J. Eng. Mech.*, **139**(5), 635-649.

Song, W. and Dyke, S. (2014), "Real-time dynamic model updating of a hysteretic structural system", *J. Struct. Eng.*, **140**(3), 04013082-04013081-04013014.

Song, X., Ahmadian, M. and Southward, S.C. (2005), "Modeling magnetorheological dampers with application of nonparametric approach", *J. Intel. Mat. Syst. Str.*, **16**(5), 421-432.

Spencer Jr., B.F., Dyke, S.J., Sain, M.K. and Carlson, J.D. (1997), "Phenomenological model for magnetorheological dampers", *J. Eng. Mech.*, **123**(3), 230-238.

Spencer Jr., B.F. and Nagarajaiah, S. (2003), "State of the art of structural control", *J. Struct. Eng.*, **129**(7), 845-856.

Stanway, R., Sproston, J. and Stevens, N. (1987), "Non-linear modeling of an electro-rheological vibration damper", *J. Electrostat.*, **20**(2), 167-184.

Van der Merwe, R. and Wan, E. (2003), "Gaussian mixture sigma-point particle filters for sequential pProbabilistic inference in dynamic state-space models", *Proceedings of the IEEE International Conference on Acoustics, Speech and Signal Processing (ICASSP)*, Hong Kong.

Wereley, N. and Pang, L. (1998), "Nondimensional analysis of semi-active electrorheological and magnetorheological dampers using approximate parallel plate models", *Smart Mater. Struct.*, **7**, 732-743.

Wu, B. and Wang, T. (2014), "Model updating with constrained unscented Kalman filter for hybrid testing", *Smart Struct. Syst.*, **14**(6), 1105-1129.

Wu, M. and Smyth, A.W. (2007), "Application of the unscented kalman filter for real-time nonlinear structural system identification", *Struct. Control Health.*, **14**, 971-990.

Wu, M. and Smyth, A. (2008), "Real-time parameter estimation for degrading and pinching hysteretic models", *Int. J. Non-linear Mech.*, **43**(9), 822-833.

Yang, G. (2001), “Large-scale magnetorheological fluid damper for vibration mitigation: modeling, testing and control”, Ph.D. Dissertation, Notre Dame University, Indiana.

Yang, J.N., Lin, S., Huang, H. and Zhou, L. (2006), “An adaptive extended kalman filter for structural damage identification”, *Struct. Control Health.*, **13**(4), 849-867.

Yao, J.T.P. (1972), “Concept of structural control”, *J. Struct. Div.*, **98**(7), 1567-1574.

Yun, C.B. and Shinozuka, M. (1980), “Identification of nonlinear structural dynamic systems”, *J. Struct. Mech.*, **8**(2), 187-203.

BS